Dayside temperature maps of the upper mesosphere and lower thermosphere of Mars retrieved from MAVEN IUVS observations of O I 297.2 nm emission

J. S. Evans[1], E. Soto[1], S. K. Jain[2], J. Deighan[2], M. H. Stevens[3], M. S. Chaffin[2], D. Y. Lo[4], S. Gupta[2], N. M. Schneider[2], and S. Curry[5]

[1]Computational Physics, Inc., Springfield, Virginia, USA
[2]Laboratory for Atmospheric and Space Physics, University of Boulder, CO, USA
[3]Space Sciences Division, U.S. Naval Research Laboratory, Washington, D.C., USA
[4]Climate and Space Sciences and Engineering, University of Michigan, Ann Arbor, MI, USA
[5]Space Sciences Laboratory, University of California Berkeley, 7 Gauss Way, Berkeley, CA 94720, USA

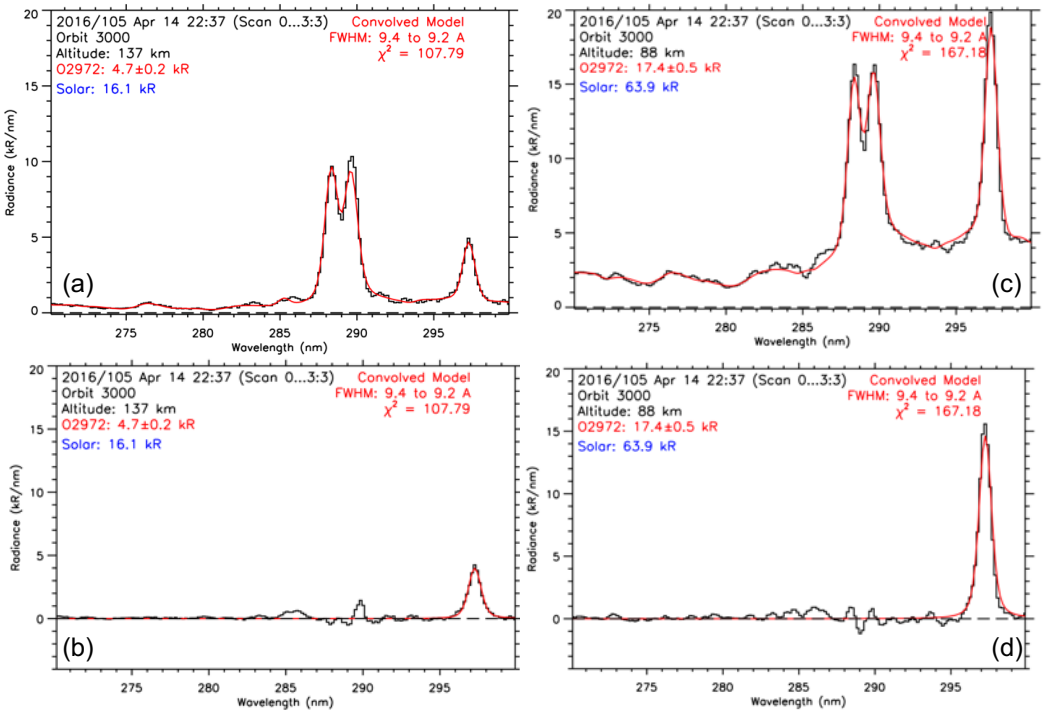

Figure S1. (a) An example composite fit (red) to an IUVS MUV spectrum (black) for a tangent altitude of 137 km. The composite fit is the sum of a solar background contribution, CO_2^+ UVD, and O I 297.2 nm emissions. (b) Residual spectrum at 137 km tangent altitude (black) obtained by subtracting the fitted solar background and CO_2^+ UVD emission from the observed spectrum and a fit to the residual spectrum (red) that is used to obtain the observed O I 297.2 nm brightness. (c)-(d) Same as (a)-(b) but for a tangent altitude of 88 km.

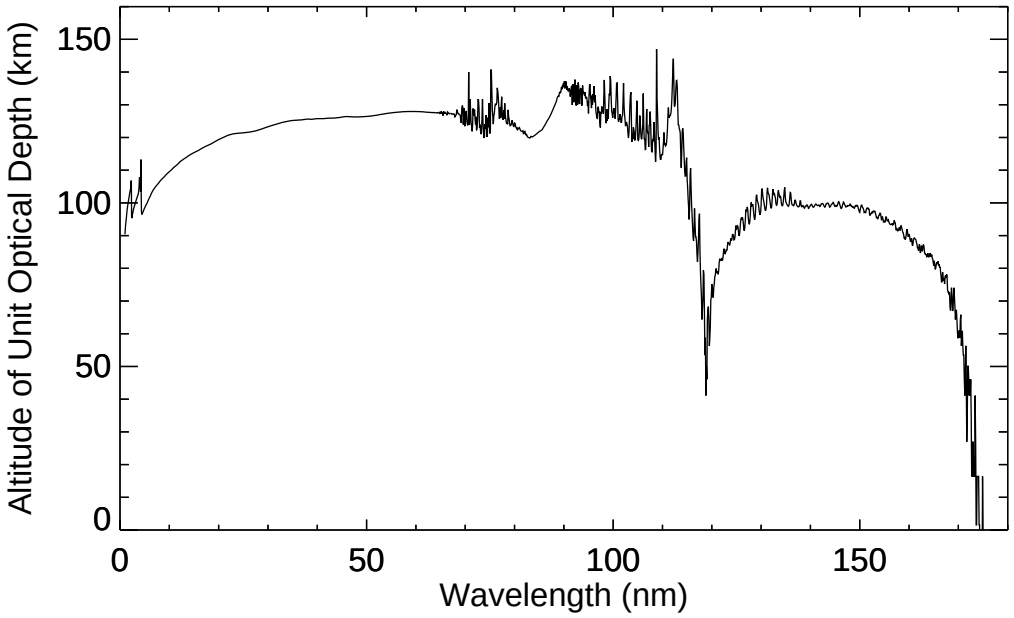

Figure S2. Altitude of unit optical depth for absorption by CO_2. The vertical column abundance is obtained from the mean CO_2 density from MCD (Millour et al., 2018) sampled over a full Martian year for an SZA of 0°. The absorption cross section is from Venot et al. (2018).

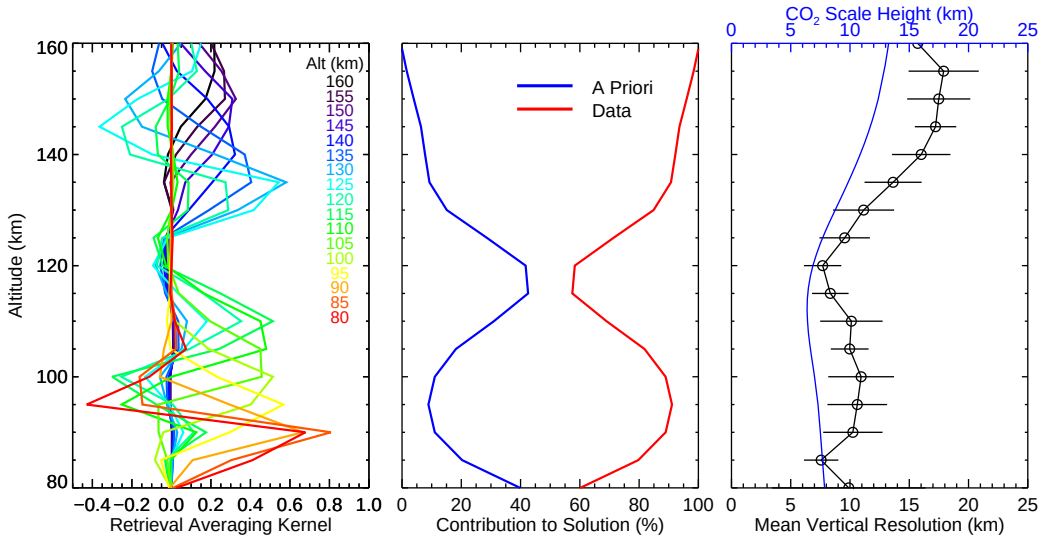

Figure S3. Left: Retrieval averaging kernel rows corresponding to the retrieval for the 9^{th} scan of periapse orbit 3000 shown in Figure 2. Middle: Mean percent contribution to retrieval solution (see Section 5.1) from *a priori* assumption (blue) and IUVS data (red) for all scans of orbit 3000. Right: Mean full-width-half-maximum (FWHM) of the averaging kernel rows for all scans of orbit 3000, which we interpret as the retrieval vertical resolution. The horizontal lines represent 1-σ natural variability of the FWHM. The mean vertical resolution from 80 to 160 km is 12 km with a standard deviation of 3.5 km. For reference, the approximate CO_2 scale height is shown in blue.

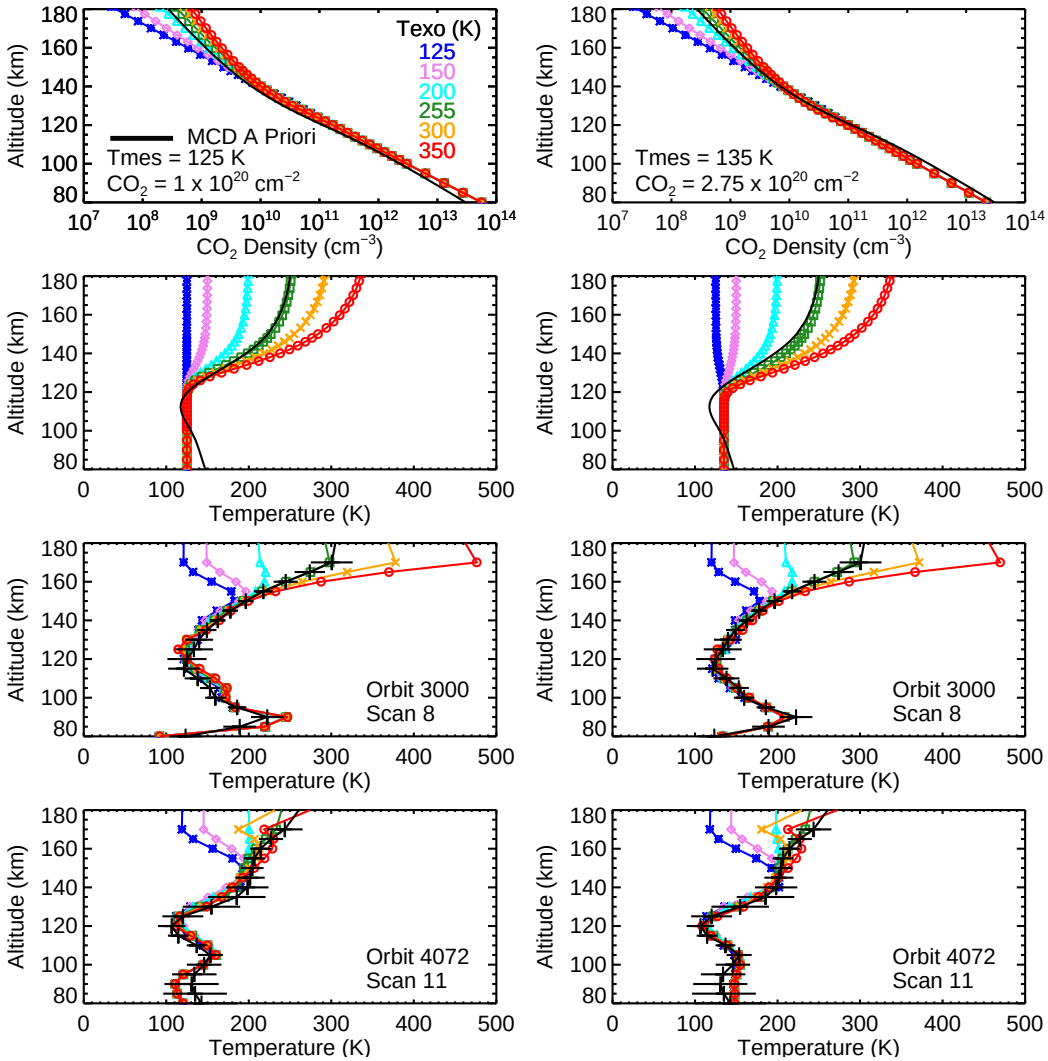

Figure S4. Top left: Alternative *a priori* CO_2 density profiles generated with J. Deighan's one dimensional photochemistry model (see Supporting Information for Evans et al., 2022) using the exospheric temperatures shown in the legend, mesospheric temperature 125 K, reference CO_2 column density for middle atmosphere bootstrapping 1 x 10^{20} cm^{-2}, N_2 mixing ratio 2.6 x 10^{-2}, Ar mixing ratio 1.9 x 10^{-2}, Eddy diffusion coefficient 2 x 10^{13} cm^2 s^{-1}, top of the atmosphere CO_2 photolysis rate 3 x 10^{-7} s^{-1}, and cross section for exponential factor 5 x 10^{-17} cm^2. The solid black curve is the MCD *a priori* CO_2 density used for the retrievals discussed in the main text. Top right: Alternative *a priori* CO_2 density profiles generated with J. Deighan's one dimensional photochemistry model using the same model parameter values as in the top left except for mesospheric temperature 135 K and reference CO_2 column density 2.75 x 10^{20} cm^{-2}. Second row: *A priori* temperatures that correspond to the alternative *a priori* CO_2 density profiles shown in the top row. Third row left: Derived temperatures calculated from CO_2 densities retrieved from the eighth scan of periapse orbit 3000 using the *a priori* density profiles shown in the top left. The black horizontal lines are the $\pm$ 1-σ uncertainties of the derived temperatures. Third row right: Derived temperatures calculated from CO_2 densities retrieved for the eighth scan of periapse orbit 3000 using the *a priori* density profiles shown in the top right. Bottom: Same as the third row but for the eleventh scan of orbit 4072.

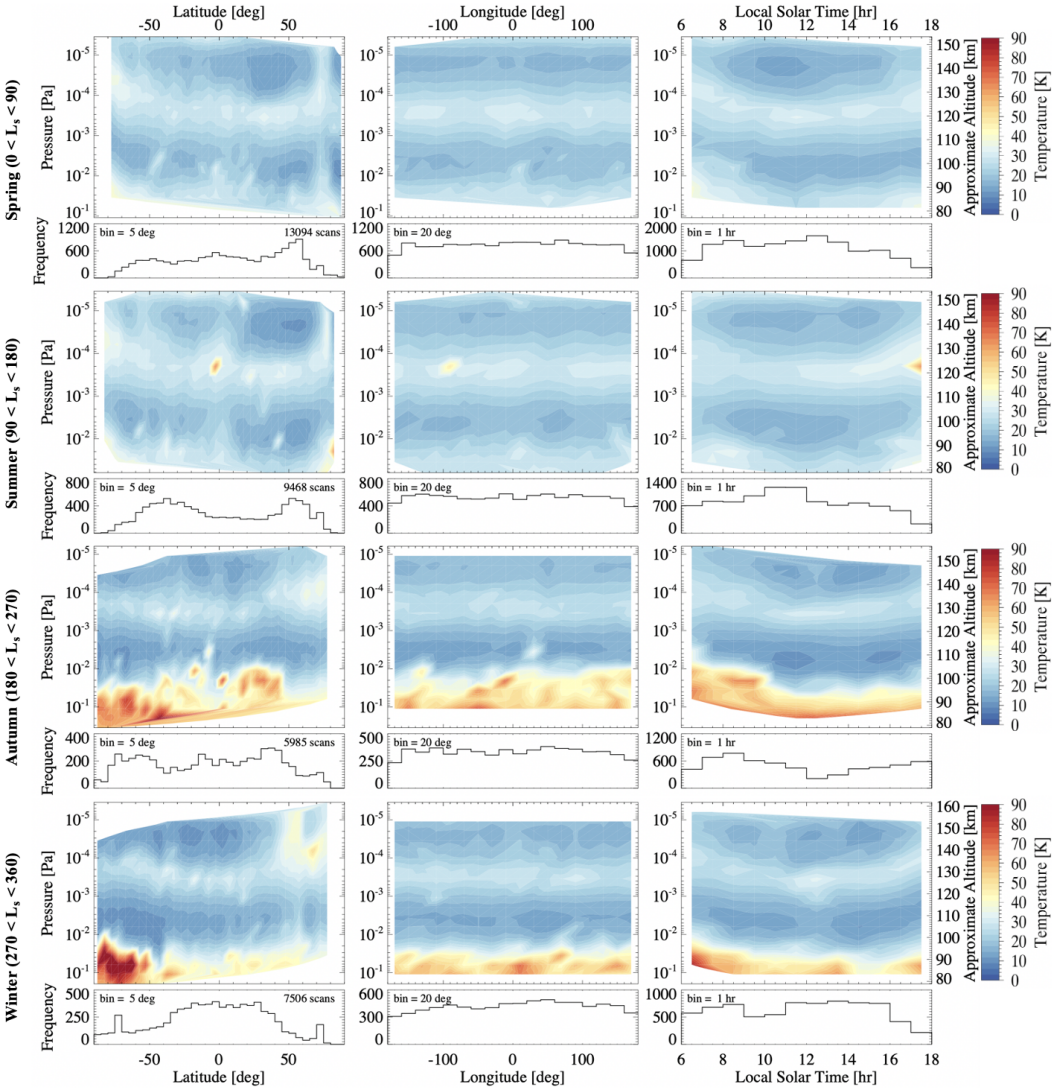

Figure S5. Uncertainties of the binned temperatures shown in Figure 7. The uncertainties are calculated as the square root of the sum of temperature variances in each bin divided by the number of samples in each bin.

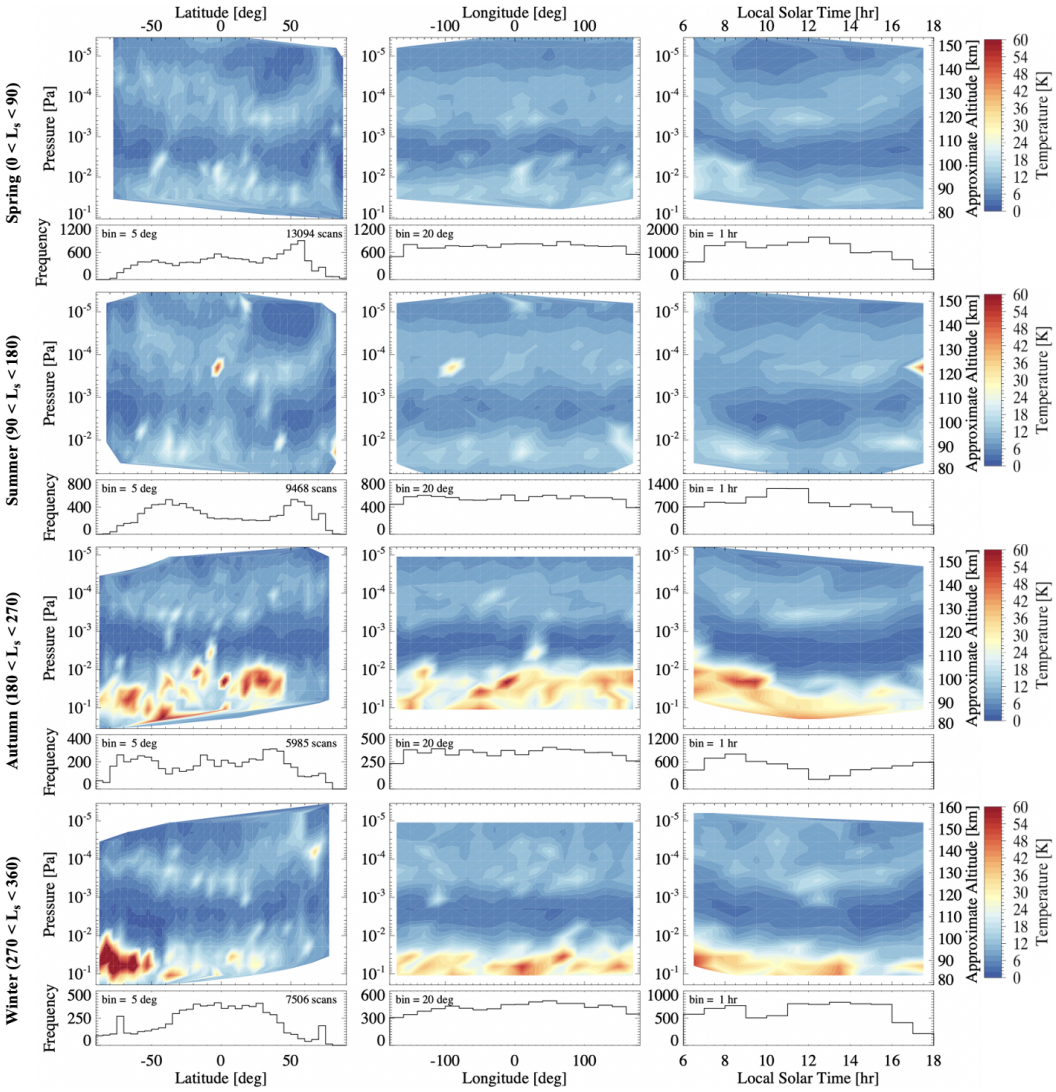

Figure S6. Standard deviation of the temperature uncertainties corresponding to the binned temperatures shown in Figure 7.

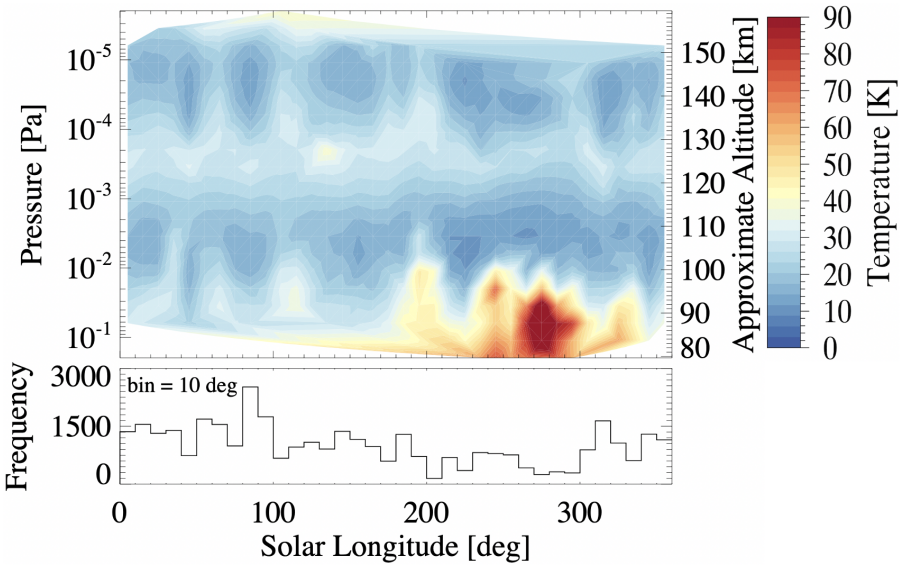

Figure S7. Uncertainties of the binned temperatures shown in Figure 12. The uncertainties are calculated as the square root of the sum of temperature variances in each bin divided by the number of samples in each bin.

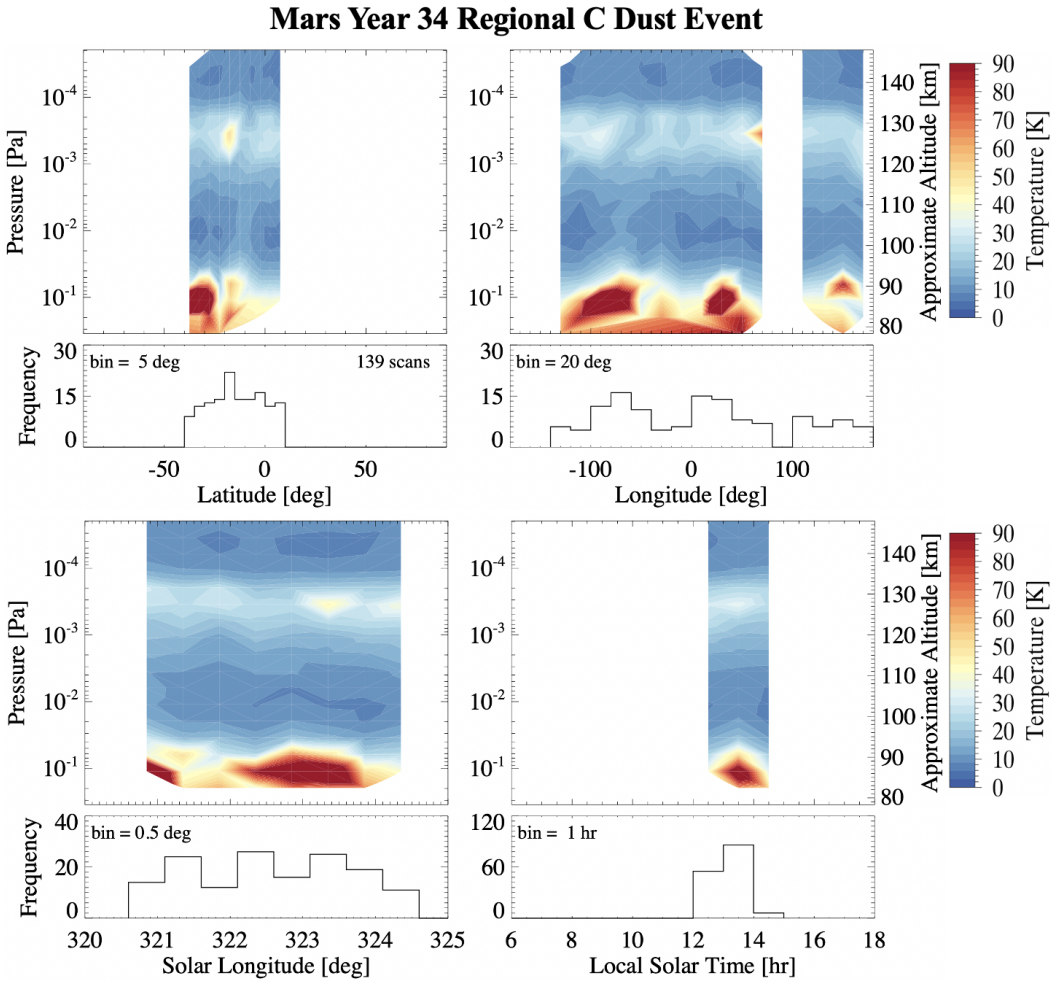

Figure S8. Uncertainties of the binned temperatures shown in Figure 13. The uncertainties are calculated as the square root of the sum of temperature variances in each bin divided by the number of samples in each bin.

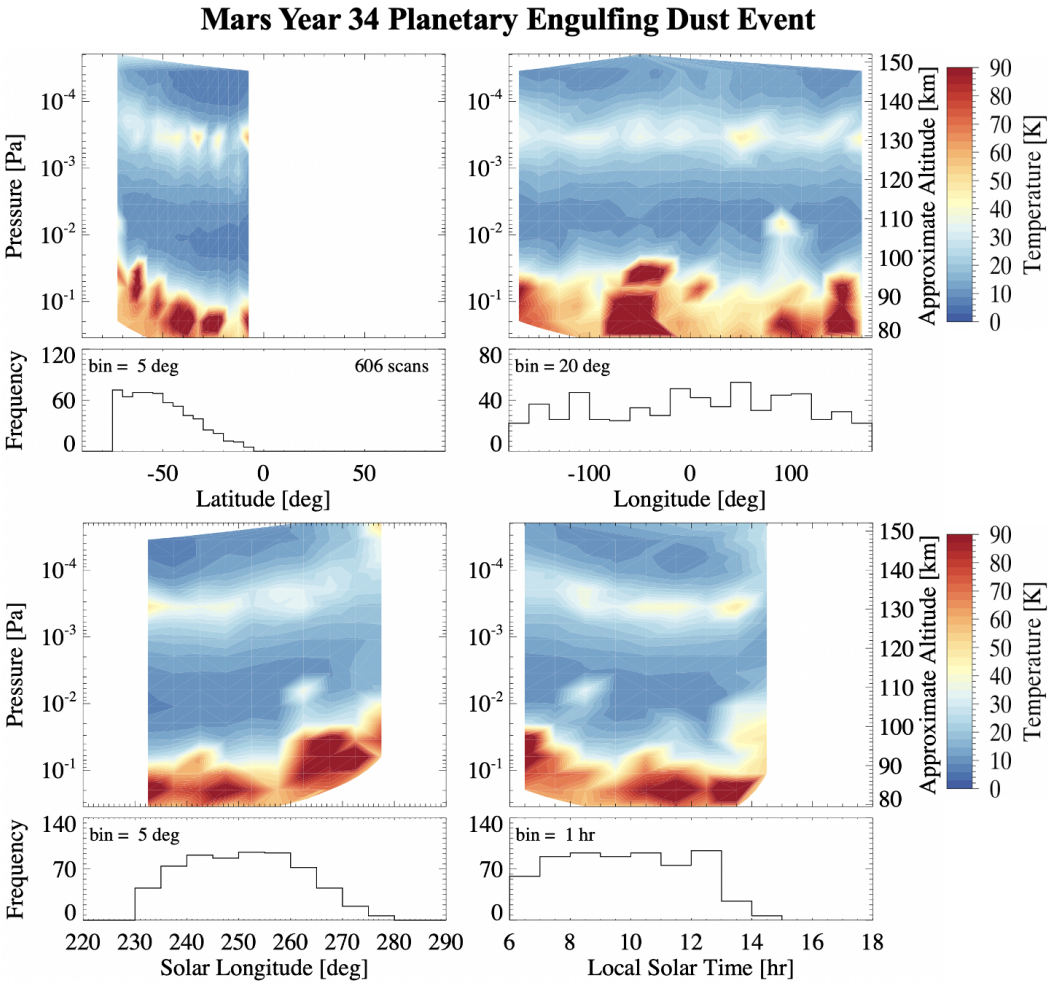

Figure S9. Uncertainties of the binned temperatures shown in Figure 14. The uncertainties are calculated as the square root of the sum of temperature variances in each bin divided by the number of samples in each bin.